Identification of Conical Structures in Small Aluminum Oxide Clusters: Infrared Spectroscopy of $(Al_2O_3)_{1-4}(AlO)^+$

Gabriele Santambrogio,[†,‖] Ewald Janssens,[†] Shaohui Li,[†] Torsten Siebert,[†]
Gerard Meijer,[‡] Knut R. Asmis,*[,‡] Jens Döbler,[§] Marek Sierka,[§] and
Joachim Sauer*[,§]

*Institut für Experimentalphysik, Freie Universität Berlin, Arnimallee 14, 14195 Berlin, Germany,
Fritz-Haber-Institut der Max-Planck-Gesellschaft, Faradayweg 4-6, 14195 Berlin, Germany, and
Institut für Chemie der Humboldt Universität zu Berlin, Unter den Linden 6,
10099 Berlin, Germany*

Received July 7, 2008; E-mail: asmis@fhi-berlin.mpg.de; js@chemie.hu-berlin.de

Abstract: The vibrational spectroscopy of the electronically closed-shell $(Al_2O_3)_n(AlO)^+$ cations with $n = 1-4$ is studied in the $530-1200$ cm^{-1} range by infrared predissociation spectroscopy of the corresponding ion–He atom complexes in combination with quantum chemical calculations. In all cases we find, assisted by a genetic algorithm, global minimum structures that differ considerably from those derived from known modifications of bulk alumina. The $n = 1$ and $n = 4$ clusters exhibit an exceptionally stable conical structure of C_{3v} symmetry, whereas for $n = 2$ and $n = 3$, multiple isomers of lower symmetry and similar energy may contribute to the recorded spectra. A blue shift of the highest energy absorption band is observed with increasing cluster size and attributed to a shortening of Al–O bonds in the larger clusters. This intense band is assigned to vibrational modes localized on the rim of the conical structures for $n = 1$ and $n = 4$ and may aid in identifying similar, highly symmetric structures in larger ions.

Introduction

Understanding how the properties of a chemical compound change with size, i.e., when passing from small molecules over nanosized clusters and thin films to the bulk solid, is not only of fundamental interest to chemistry, but also represents a prerequisite for designing materials with tailored properties. Among metal oxides, aluminum oxides are of particular interest, because they are widely used in industrial applications, for example, as ceramics, coatings, soft abrasives, absorbents and supports for catalysts.[1] They also show a remarkable structural diversity in the solid state. Next to the thermodynamically most stable form of alumina, α-Al$_2$O$_3$ (corundum), there exist many metastable A$_2$O$_3$ polymorphs, the so-called transition aluminas. Due to poorly developed crystallinity as well as surface reconstruction, which limits the applicability of advanced surface analytical techniques to probe such small scale and irregular structures, their detailed structural characterization remains problematic.[2,3] This, together with recent advances in the synthesis of aluminum oxide microtubes,[4] nanosheets[5] and

-fibers,[6] stimulates the development and application of alternative characterization techniques for structures of finite aluminum oxide particles at the nanometer scale.

Evidence that α-alumina is not the most stable phase for nanostructured alumina is derived from studies on the vibrational spectroscopy of aluminum oxide films and clusters. The infrared (IR) spectra of thin Al$_2$O$_3$ films[7–9] contain clear and distinct features caused by lattice vibrations that were assigned to a γ-Al$_2$O$_3$ crystalline structure. More recently, the structure of an ultrathin alumina film on NiAl was found to be different from known bulk alumina structures.[10]

Similarly, IR resonance-enhanced multiphoton ionization (REMPI) studies[11,12] on neutral AlO(Al$_2$O$_3$)$_n$ clusters ($5 \le n \le 70$) in the gas phase suggest γ-Al$_2$O$_3$-type structures up to $n = 34$, while the IR-REMPI spectra of the larger clusters closely resemble that of amorphous aluminum oxide. A more detailed structural assignment to individual cluster structures proved to be difficult, mainly due to the lack of mass-selectivity prior to IR irradiation in these types of experiments.

† Institut für Experimentalphysik, Freie Universität Berlin.
‡ Fritz-Haber-Institut der Max-Planck-Gesellschaft.
§ Institut für Chemie der Humboldt Universität zu Berlin.
‖ Present address: East Tokyo Laboratory, Genesis Research Institute, Inc., 717-86 Futamata, Ichikawa, Chiba 272-0001, Japan.

(1) Hart, L. D. *Alumina Chemicals: Science and Technology Handbook*; The American Ceramic Society: New York, 1990.
(2) Tsybulya, S. V.; Kryukova, G. N. *Phys. Rev. B* **2008**, *77*.
(3) Levin, I.; Brandon, D. *J. Am. Ceram. Soc.* **1998**, *81*, 1995–2012.
(4) Peng, Q.; Sun, X. Y.; Spagnola, J. C.; Hyde, G. K.; Spontak, R. J.; Parsons, G. N. *Nano Lett.* **2007**, *7*, 719–722.
(5) Ma, C.; Chang, Y.; Ye, W.; Shang, W.; Wang, C. *J. Colloid Interface Sci.* **2008**, *317*, 148–154.

(6) Zhang, M.; Zhang, R.; Xi, G. C.; Liu, Y.; Qian, Y. T. *J. Nanosci. Nanotechnol.* **2006**, *6*, 1437–1440.
(7) Franchy, R. *Surf. Sci. Rep.* **2000**, *38*, 199–294.
(8) Frank, M.; Wolter, K.; Magg, N.; Heemeier, M.; Kuhnemuth, R.; Bäumer, M.; Freund, H. J. *Surf. Sci.* **2001**, *492*, 270–284.
(9) Lee, M. B.; Lee, J. H.; Frederick, B. G.; Richardson, N. V. *Surf. Sci.* **2000**, *448*, L207–L212.
(10) Kresse, G.; Schmid, M.; Napetschnig, E.; Shishkin, M.; Köhler, L.; Varga, P. *Science* **2005**, *308*, 1440–1442.
(11) Demyk, K.; van Heijnsbergen, D.; von Helden, G.; Meijer, G. *Astron. Astrophys.* **2004**, *420*, 547–552.
(12) van Heijnsbergen, D.; Demyk, K.; Duncan, M. A.; Meijer, G.; von Helden, G. *Phys. Chem. Chem. Phys.* **2003**, *5*, 2515–2519.

Mass-selective experiments, which are difficult for neutral clusters, can be readily performed on cluster ions. While ionic systems can exhibit structures and properties that differ from their neutral counterparts, they do present a pathway to a systematic study of the structural and electronic properties as a function of size. This yields important benchmark data for the more approximate theoretical models applied to the characterization of surfaces. Previous experimental studies on aluminum oxide cluster ions include mass spectrometry,[13] characterization of their reactivity,[14–20] ionization potentials (via charge transfer reactions),[21] magnetic properties,[22] as well as photoelectron[23,24] and IR[25] spectroscopy. Wang et al.[23,24] measured photoelectron spectra of the gas phase $Al_{1-3}O_{1-5}^{-}$ clusters. On the basis of partially vibrationally resolved photoelectron spectra the ground and excited electronic states of the corresponding neutral aluminum oxide clusters were assigned, resolving several conflicting assignments from previous low-temperature matrix isolation studies (see ref 26 and references therein).

Many computational studies have been performed on aluminum oxide clusters. In several studies,[27–31] Al_8O_{12} is assumed to exhibit a bulk-like structure and is used as a model for bulk and surface α-Al_2O_3. Other studies[32,33] predict highly symmetric caged structures, including a cubic O_h structure for Al_8O_{12}. However, Sierka et al.[25] have shown that neither the bulk-like nor the caged structure represents the global energy minimum on the potential energy surface. An unexpected structure of lower symmetry was identified for $Al_8O_{12}^{+}$ by combining IR multiple photon dissociation (MPD) spectroscopy with a global minimum search strategy in DFT. These results clearly show that aluminum oxide clusters can exhibit nonintuitive structures, whose identification requires (i) a combined experimental/computational approach and (ii) a global optimization scheme for identifying low-energy structural candidates.

Here, we report on the vibrational spectra of aluminum oxide cluster ions and study the structural evolution of $(Al_2O_3)_{1-4}(AlO)^{+}$ cations as a function of size. We have chosen the $(Al_2O_3)_n(AlO)^{+}$ series, because these clusters were found to be particularly stable,[12] presumably due to their closed electronic valence shell. This is in contrast to the $(Al_2O_3)_n^{\pm}$ radical ions with an uneven number of valence electrons, among which is the previously studied $Al_8O_{12}^{+}$.[25] The comparison of the IR vibrational predissociation (VPD) spectra of the corresponding ion–He atom complexes with simulated linear absorption spectra leads to a reliable identification of the geometric and electronic structure of the cluster ions, from which structural motifs and binding information are extracted.

Experimental Section

The experiments are carried out on a previously described tandem mass spectrometer–ion trap system,[34] installed at the FELIX user facility of the FOM Instituut Rijnhuizen.[35] Aluminum oxide clusters are prepared by a pulsed laser vaporization source operated at 10 Hz. The plasma-containing aluminum atoms are entrained in a pulse of 1% O_2 seeded in He carrier gas, expanded through a clustering channel and passed through a 2 mm diameter skimmer. All cluster cations are collimated and thermalized to room temperature by collisions with Ar atoms in a radio frequency (RF) decapole ion guide. The ions are then mass-selected with a first quadrupole mass filter and accumulated in an RF He-filled (~0.007 mbar) hexadecapole ion trap, where they are thermalized by inelastic collisions with the He buffer gas.

At sufficiently low ion trap temperatures (20 K), we observed the formation of aluminum oxide ion complexes with He and H_2. These weakly bound complexes are used to perform infrared vibrational predissociation (IRVPD) experiments.[36] The absorption of a few and often only a single IR photon(s) by the parent ion is already sufficient for vibrational predissociation and loss of the messenger species M, i.e.,

$$(Al_2O_3)_n(AlO)^{+} \cdot M \xrightarrow{h\nu} (Al_2O_3)_n(AlO)^{+} + M, \quad (1)$$

where M represents one or multiple He atoms (or H_2 molecules). IRVPD spectra are obtained by photoexcitation of the trapped ions with pulsed radiation from the "Free Electron Laser for Infrared eXperiments" FELIX,[35] which is operated at 5 Hz and applied collinear to the ion trap main axis. Directly after FELIX fires all ions are extracted from the trap and detected mass-selectively. We obtain the IRVPD spectrum by monitoring the messenger complex of the parent ion, i.e., photoabsorption manifests itself as a dip in the ion signal (depletion spectra). First, overview spectra are recorded with a 0.1-μm step size to identify the absorption regions. The region of interest is then scanned with higher resolution and the appropriate laser attenuation in order to avoid saturation. The stability in the production of aluminum oxide ions by laser vaporization was on the order of ±10% of the signal, leading to

(13) King, F. L.; Dunlap, B. I.; Parent, D. C. *J. Chem. Phys.* **1991**, *94*, 2578–2587.
(14) Gianotto, A. K.; Rawlinson, J. W.; Cossel, K. C.; Olson, J. E.; Appelhans, A. D.; Groenewold, G. S. *J. Am. Chem. Soc.* **2004**, *126*, 8275–8283.
(15) Jarrold, M. F.; Bower, J. E. *J. Chem. Phys.* **1986**, *85*, 5373–5375.
(16) Jarrold, M. F.; Bower, J. E. *J. Chem. Phys.* **1987**, *87*, 5728–5738.
(17) Ruatta, S. A.; Hanley, L.; Anderson, S. L. *Chem. Phys. Lett.* **1987**, *137*, 5–9.
(18) Scott, J. R.; Groenewold, G. S.; Gianotto, A. K.; Benson, M. T.; Wright, J. B. *J. Phys. Chem. A* **2000**, *104*, 7079–7090.
(19) Johnson, G. E.; Tyo, E. C.; Castleman, A. W. *J. Phys. Chem. A* **2008**, *112*, 4732–4735.
(20) Feyel, S.; Döbler, J.; Hökendorf, R.; Beyer, M. K.; Sauer, J.; Schwarz, H. *Angew. Chem., Int. Ed.* **2008**, *47*, 1946–1950.
(21) Bach, S. B. H.; McElvany, S. W. *J. Chem. Phys.* **1991**, *95*, 9091–9094.
(22) Cox, D. M.; Trevor, D. J.; Whetten, R. L.; Rohlfing, E. A.; Kaldor, A. *J. Chem. Phys.* **1986**, *84*, 4651–4656.
(23) Desai, S. R.; Wu, H. B.; Rohlfing, C. M.; Wang, L.-S. *J. Chem. Phys.* **1997**, *106*, 1309–1317.
(24) Wu, H. B.; Li, X.; Wang, X. B.; Ding, C. F.; Wang, L.-S. *J. Chem. Phys.* **1998**, *109*, 449–458.
(25) Sierka, M.; Döbler, J.; Sauer, J.; Santambrogio, G.; Brümmer, M.; Wöste, L.; Janssens, E.; Meijer, G.; Asmis, K. R. *Angew. Chem., Int. Ed.* **2007**, *46*, 3372–3375.
(26) Andrews, L.; Burkholder, T. R.; Yustein, J. T. *J. Chem. Phys.* **1992**, *96*, 10182–10189.
(27) Fernandez, E. M.; Eglitis, R.; Borstel, G.; Balbas, L. C. *Phys. Status Solidi B* **2005**, *242*, 807–809.
(28) Magg, N.; Immaraporn, B.; Giorgi, J. B.; Schroeder, T.; Bäumer, M.; Döbler, J.; Wu, Z. L.; Kondratenko, E.; Cherian, M.; Baerns, M.; Stair, P. C.; Sauer, J.; Freund, H.-J. *J. Catal.* **2004**, *226*, 88–100.
(29) Sauer, J.; Döbler, J. *Dalton Trans.* **2004**, *19*, 3116–3121.
(30) Sawilowsky, E. F.; Meroueh, O.; Schlegel, H. B.; Hase, W. L. *J. Phys. Chem. A* **2000**, *104*, 4920–4927.
(31) Wittbrodt, J. M.; Hase, W. L.; Schlegel, H. B. *J. Chem. Phys. B* **1998**, *102*, 6539–6548.
(32) Linnolahti, M.; Pakkanen, T. A. *Inorg. Chem.* **2004**, *43*, 1184–1189.
(33) Sun, J.; Lu, W. C.; Zhang, W.; Zhao, L. Z.; Li, Z. S.; Sun, C. C. *Inorg. Chem.* **2008**, *47*, 2274–2279.

(34) Asmis, K. R.; Brümmer, M.; Kaposta, C.; Santambrogio, G.; von Helden, G.; Meijer, G.; Rademann, K.; Wöste, L. *Phys. Chem. Chem. Phys.* **2002**, *4*, 1101–1104.
(35) Oepts, D.; van der Meer, A. F. G.; van Amersfoort, P. W. *Infrared Phys. Technol.* **1995**, *36*, 297–308.
(36) Brümmer, M.; Kaposta, C.; Santambrogio, G.; Asmis, K. R. *J. Chem. Phys.* **2003**, *119*, 12700.

small variations in the parent ion signal baseline of the IRVPD spectra.

Computational Section

All calculations are performed using the TURBOMOLE program package.[37,38] Global optimizations of the cluster structures at the DFT level use the B3-LYP[39,40] exchange correlation functional and split valence plus polarization (SVP) basis sets.[41] We apply our own implementation of the genetic algorithm[25] closely following the original procedure developed by Deaven and Ho.[42] Each run consists of 50 generations with 16 parent and 8 children structures per generation. For $Al_3O_4^+$, $Al_5O_7^+$, and $Al_7O_{10}^+$ global minimizations including the He messenger atoms were performed. For $Al_9O_{13}^+$, the global minimum was calculated without a He atom. It was attached to the global minimum structure afterward. In the case of $Al_7O_{10} \cdot He^+$, the convergence of the genetic algorithm is poorer due to a high number of structures with similar energies. In this case, an additional run with 50 parents and 25 children was performed to ensure convergence.

For all structures, final structure optimizations are performed using the B3-LYP functional along with triple-ζ valence plus polarization (def2-TZVP)[43] basis sets on all atoms. The calculations yield stable wave functions, characterized by a large gap between the highest occupied and lowest unoccupied orbital so that triplet states can be safely excluded as possible ground states.

For the global minimum structure of each species and energetically close isomers frequency calculations were performed within the harmonic approximation using analytical second derivatives. Simulated stick spectra are determined from the unscaled calculated vibrational frequencies, using intensities calculated in the harmonic approximation from analytical derivatives of the dipole moment and then convoluted using a Gaussian line shape function.

For $Al_5O_7^+ \cdot He_2$ and $Al_7O_{10}^+ \cdot He$ additional calculations using second order perturbation theory[44] (MP2) were performed with the RICC2 module of Turbomole using the resolution of identity method.[45] For $Al_5O_7^+ \cdot He_2$-coupled cluster calculations with single and double excitations and pertubative triple excitations CCSD(T) were performed with Molpro 2006.1.[46] These calculations are single point calculations at the MP2/def2-TZVP structures and employ either the def2-QZVP[47] or cc-pVQZ[48,49] basis sets. The T1 diagnostics does not provide any indication of a possible multi-reference character.

Results and Discussion

Nature of the Observed Complexes. Figure 1 shows the mass spectra obtained by scanning the second mass filter after trapping mass-selected $(Al_2O_3)_n(AlO)^+$ parent ions, previously mass-selected with the first mass filter, for up to 100 ms and then extracting all ions from the ion trap. The largest peak in each spectrum corresponds to the (bare) parent ion and is labeled "Parent" on the mass axis. Additional peaks are observed at
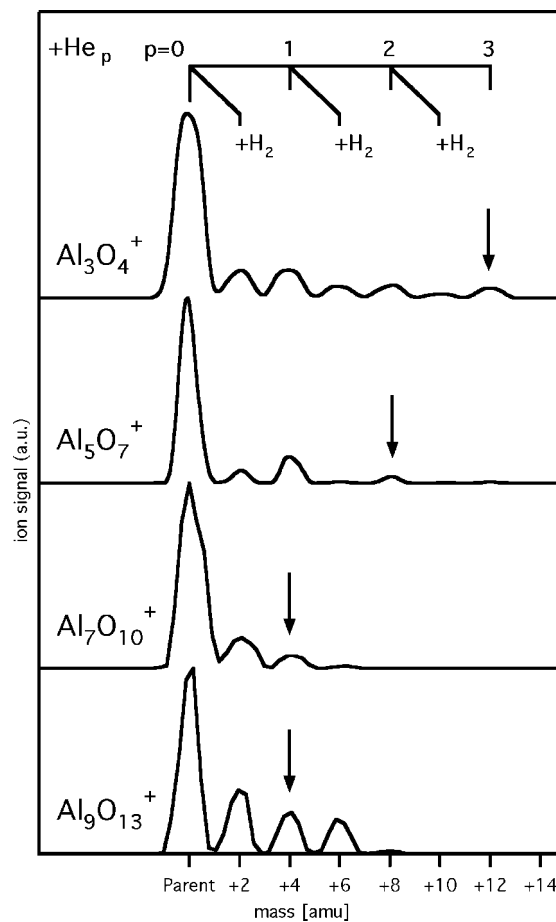
(37) Ahlrichs, R.; Bär, M.; Häser, M.; Horn, H.; Kölmel, C. *Chem. Phys. Lett.* **1989**, *162*, 165–169.
(38) Treutler, O.; Ahlrichs, R. *J. Chem. Phys.* **1995**, *102*, 346–354.
(39) Becke, A. D. *J. Chem. Phys.* **1993**, *98*, 5648–5652.
(40) Lee, C.; Yang, W.; Parr, R. G. *Phys. Rev. B* **1988**, *37*, 785–789.
(41) Schäfer, A.; Horn, H.; Ahlrichs, R. *J. Chem. Phys.* **1992**, *97*, 2571–2577.
(42) Deaven, D. M.; Ho, K. M. *Phys. Rev. Lett.* **1995**, *75*, 288–291.
(43) Weigend, F.; Ahlrichs, R. *Phys. Chem. Chem. Phys.* **2005**, *7*, 3297–3305.
(44) Møller, C.; Plesset, M. S. *Phys. Rev.* **1934**, *46*, 618–622.
(45) Hättig, C.; Weigend, F. *J. Chem. Phys.* **2000**, *113*, 5154–5161.
(46) Werner, H.-J. et al., MOLPRO package of Ab Initio Programs, 2006.
(47) Weigend, F.; Furche, F.; Ahlrichs, R. *J. Chem. Phys.* **2003**, *119*, 12753–12762.
(48) Dunning, T. H. *J. Chem. Phys.* **1989**, *90*, 1007–1023.
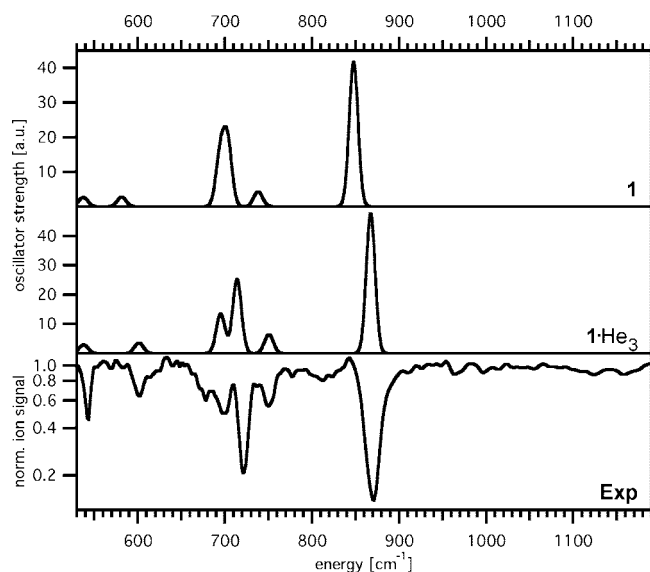(49) Woon, D. E.; Dunning, T. H. *J. Chem. Phys.* **1993**, *98*, 1358–1371.

Figure 1. Mass spectra obtained by scanning the second mass filter after trapping mass-selected $(Al_2O_3)_n(AlO)^+$ clusters (parent ions) with $n = 1-4$ (top to bottom) for up to 100 ms at 20 K and ~0.007 mbar He pressure and then extracting all ions from the ion trap. For an easier comparison, all mass spectra are aligned to the mass of the corresponding parent ion, which is initially mass-selected using the first mass filter. The mass channels, which are used to monitor the IRVPD spectra, are indicated by arrows.

higher masses. These are assigned to complexes of the parent ion with He atoms, H_2 molecules or both (see also ref 36). Traces of H_2 gas—the main component of rest gas degassing from the vacuum chamber walls—is also present in the trap region. Even though H_2 is present at much lower concentrations than He, it competes in the formation of the complexes due to its higher polarizability and presence of a quadrupole moment, resulting in a higher binding energy to the ion. The presence of H_2 makes the assignment of the mass spectra less straightforward, because $2m(H_2) \approx m(He)$, where m represents the mass of the corresponding messenger species. However, for $n = 1$ and $n = 2$ the intensity distribution clearly suggests a dominant $\Delta m = 4$ progression, labeled with $p = 0-3$ in Figure 1, upon which a weaker $\Delta m = 2$ progression is superimposed. This suggests the predominant formation of pure He-atom complexes for the $\Delta m = 4$ progression, with only minor contributions from complexes containing (at least) two H_2 molecules. However, for $n = 3$ and $n = 4$ there may indeed be a significant contribution to the $p = 1$ mass peak from the complex containing two H_2 molecules. In order to minimize the contribution from complexes with larger mass decaying into the monitored mass channel, which could mask the depletion signal, IRVPD spectra are measured by monitoring the depletion of the peak corresponding to the complex with the largest number of He atoms observed in the mass spectra of sufficient signal,

Figure 2. Comparison of experimental IRVPD spectrum of $Al_3O_4^+ \cdot He_3$ (**Exp**) to simulated linear absorption spectra of $Al_3O_4^+ \cdot He_3$ ($1 \cdot He_3$) and $Al_3O_4^+$ (**1**).

i.e., $p = 3$ for $n = 1$, $p = 2$ for $n = 2$, and $p = 1$ for $n = 3$ and 4 (indicated by the arrows in Figure 1). Possible contributions from complexes containing multiple H_2 molecules to the IRVPD spectra, in particular for $n = 3$ and $n = 4$, are assumed to be negligible, due to their considerably higher dissociation threshold (compared to the corresponding He-complexes).

$Al_3O_4^+$. The experimental IRVPD spectrum of $Al_3O_4^+ \cdot He_3$ is shown in Figure 2 (bottom trace). It exhibits a very strong absorption at 871 cm^{-1}, a group of four maxima around 700 cm^{-1}, and two less intense bands at 602 and 543 cm^{-1} (see Table 1 for all experimental band positions). The lowest energy structure calculated for $Al_3O_4^+$ (**1** in Figure 3) has C_{3v} symmetry and consists of a 6-membered (6m) ring of alternating Al and 2-fold coordinated O atoms and a 3-fold coordinated O atom on top of the ring. The next stable structure found by the genetic algorithm lies nearly 200 kJ/mol higher in energy and should therefore not be observed. The C_{3v} symmetry is maintained in the $Al_3O_4^+ \cdot He_3$ complex ($1 \cdot He_3$). Its calculated linear IR absorption spectrum (trace $1 \cdot He_3$ in Figure 2) is in excellent agreement with the experimental IR-PD spectrum with respect to peak positions as well as relative peak intensities. Nine vibrational modes, three of e and a_1 symmetry, contribute to the IR absorption spectrum. The highest frequency band (experiment: 871 cm^{-1}, calculation: 868 cm^{-1}), which is also the most intense, corresponds to a doubly degenerate Al–O antisymmetric stretching mode of all six atoms in the 6m ring, while the next lower band (750 cm^{-1}, 750 cm^{-1}) corresponds to the (nondegenerate) symmetric stretching mode of a_1 symmetry, mainly involving the three bridging, 2-fold coordinated O atoms. The four bands below 750 cm^{-1} result from modes that also involve the 3-fold coordinated O atom.

Comparison of the calculated spectra of $Al_3O_4^+ \cdot He_3$ and $Al_3O_4^+$ (traces $1 \cdot He_3$ and **1** in Figure 2) shows that the binding of He atoms to the cation has no effect on the 695 (a_1) and 537 cm^{-1} (e) modes because they predominantly involve displacement of the 3-fold coordinated O atom, which does not directly interact with the He atoms. In contrast, it has a pronounced effect on the four modes calculated at 848 (e), 738 (a_1), 703 (e), and 581 cm^{-1} (a_1) which are blue-shifted by +20, +11, +12, and +20 cm^{-1} with the addition of three He atoms. This

is due to a caging effect, since the presence of the He atoms hinders the displacement of the atoms comprising the 6m ring. The extent of the frequency shift is unexpected and attributed to the exceptionally high Lewis acidity of the 3-fold coordinated Al atoms, resulting in Al–He bond lengths slightly below 2 Å with a dissociation energy of 11.6 kJ/mol (B3LYP/def2-TZVP) for the loss of a He atom. The latter value is comparable to the average Al–He bond energy of 12 kJ/mol ($\sim$1000 cm^{-1}), determined from the energy difference of 36 kJ/mol between $Al_3O_4^+ \cdot He_3$ and bare $Al_3O_4^+$ (see Table S7 of the Supporting Information). The latter value is further confirmed by a CCSD(T) calculations, which yields an energy difference of 34 kJ/mol. Consequently, more than one IR photon, in the spectral range discussed here, is required to break one of these unusually strong metal-rare gas bonds.

$Al_5O_7^+$. The experimental IRVPD spectrum of $Al_5O_7^+ \cdot He_2$ (lower trace in Figure 4) is more complex and extends $\sim$100 cm^{-1} to higher energies compared to the $Al_3O_4^+ \cdot He_3$ spectrum. Three main absorption regions of similar intensity are observed at 1030–950, 880–800, and 780–680 cm^{-1}. For $Al_5O_7^+ \cdot He_2$, the calculations predict two isomers (**2A** and **2B** in Figure 3) of similar energy. **2A** is a C_s symmetric cage-like structure that consists of a quasi-planar 8m ring with alternating Al and O atoms "supporting" an AlO_3 unit. All Al atoms are in 3-fold coordination, while six O atoms are in 2-fold and one in 3-fold coordination. In contrast, **2B** is a sheet-like structure with C_2 symmetry, with four Al atoms in 3-fold and one in 4-fold coordination, while five O atoms are in 2-fold, and two in 3-fold coordination. For the basis set used in the frequency calculations (def2-TZVP) **2B** is by 3.2 kJ/mol more stable than **2A**. The difference in zero point vibrational energy is small, it favors **2B** by 1.6 kJ/mol. To check the relative stabilities of the two isomers additional calculations have been performed (see Table S8 of the Supporting Information). When using the larger def2-QZVP basis set, it is found that the stability is reversed; **2A** is now more stable by 1.2 kJ/mol (without ZPE). Wave function-based calculations support this finding. MP2/def2-QZVP yields a preference for **2A** of 0.6 kJ/mol, and CCSD(T)/def2-QZVP of 2.7 kJ/mol, so that it is reasonable to assume **2A** as the slightly more stable structure.
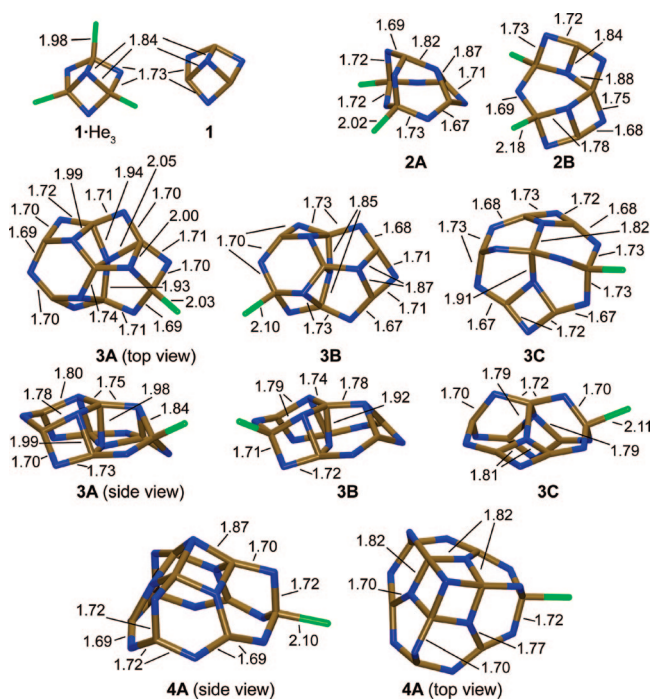
Despite the geometric differences, the calculated spectra of **2A** and **2B** (traces **2A** and **2B** in Figure 4) are rather similar; most bands are found in both spectra with very similar frequencies but different intensities. Spectrum **2A** is clearly in better agreement with the experiment and accounts for all the prominent peaks found in the experimental spectrum. This supports an assignment of structure **2A** as the global minimum. However, the presence of isomer **2B** cannot be excluded. On the contrary, if a mixture of the two isomers is postulated, which is reasonable given the small predicted energy difference, the agreement between experiment and simulation can be improved, in particular for reproducing the shoulder at 960 cm^{-1} and the features observed between 600 and 650 cm^{-1}. A 3:1 mixture of isomer **2A** to **2B** (see trace **MIX(A,B)** in Figure 4) yields the best agreement.

When the spectra of $Al_5O_7^+ \cdot He_2$ and $Al_3O_4^+ \cdot He_3$ are compared, three main differences can be seen. (i) The spectrum of $Al_5O_7^+ \cdot He_2$ is richer in features, (ii) it has additional bands at higher frequencies and (iii) the influence of the messenger atoms is less pronounced (see below). (i) A richer spectrum is expected for a larger cluster, in particular if it is of low symmetry (C_s vs C_{3v}) such that symmetry-imposed degeneracies are lifted. The position of the IR bands correlates well with the length of
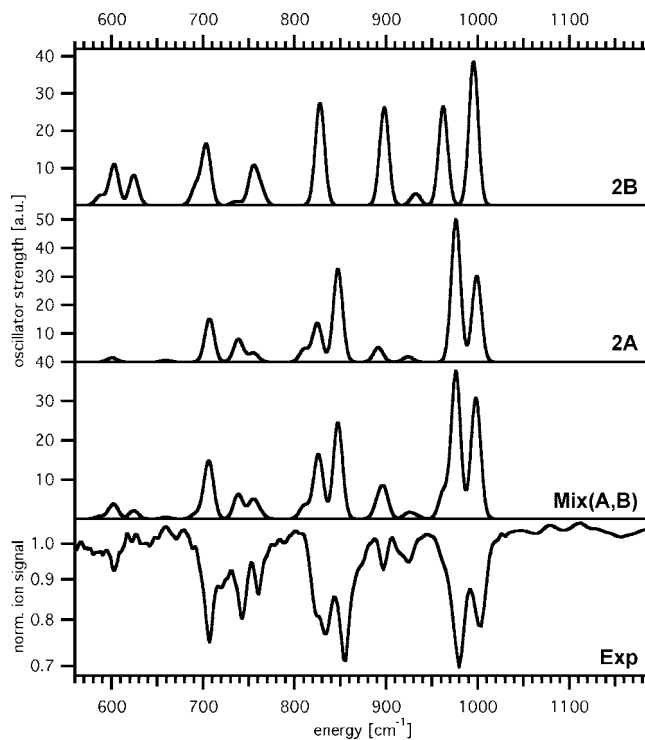
Table 1. Experimental Band Positions and Calculated Harmonic Frequencies (both in cm^{-1}), Symmetries and Intensities (in km/mol) for $(Al_2O_3)_{1-4}AlO^+ \cdot He_n{}^a$

ion	exp./theory[b]	vibrational frequencies[c]
$Al_3O_4{}^+ \cdot He_3$	experiment	871, 750, 722, 700, 678, 602, 543
	$^1A_1$ (C_{3v}), **1**·He$_3$	868 (e, 300), 755(a$_2$,0), 751(a$_1$, 81), 714 (e, 158), 695 (a$_1$, 169), 601 (a$_1$, 45), 538 (e,18)
$Al_5O_7{}^+ \cdot He_2$	experiment	1004, 980, 925, 897, 856, 834, 824(s), 761, 743, 721(s), 707, 671, 642, 604, 589(s)
	$^1A'$ (C_s), **2A**	999 (a',379), 976 (a",627), 924 (a",23), 892 (a",62), 848 (a',409), 825 (a',169), 811 (a",56), 756 (a',35), 749 (a",9), 739 (a',99), 707 (a',190), 659 (a",7), 601 (a',18), 512 (a",34), 500 (a",10)
$Al_7O_{10}{}^+ \cdot He$	experiment	1015(s), 996, 953, 916, 889, 856, 824, 769, 738, 721, 701, 673, 639, 608, 588
	^1A (C_1), **3A**	993 (a,391), 989 (a,678), 947 (a,373), 924 (a,400), 917 (a,20), 895 (a,226), 849 (a,83), 836 (a,38), 790 (a,62), 775 (a,31), 765 (a,174), 729 (a,19), 713 (a,95), 696 (a,105), 670 (a,37), 641 (a,46), 606 (a,175), 588 (a,122), 576 (a,178), 524 (a,19), 511 (a,64)
$Al_9O_{13}{}^+ \cdot He$	experiment	1029, 962(s), 935, 899, 867, 851(s), 836, 818, 798, 771, 724, 680, 631, 610, 590, 558
	$^1A'$ (C_s), **4A**	1029 (a',903), 1027 (a",879), 979 (a",1), 943 (a',566), 934 (a',177), 933 (a",171), 897 (a',164), 863 (a',154), 860 (a",137), 844 (a',116), 825 (a",1), 824 (a',1), 795 (a",131), 794 (a",146), 792 (a',263), 772 (a',225), 712 (a',5), 711 (a",6), 677 (a",127), 677 (a',131), 647 (a',27), 634 (a",0), 626 (a",77), 625 (a',66), 607 (a',316), 560 (a",83), 558 (a',82)

^{a} Only vibrational modes with harmonic frequencies above 500 cm^{-1} are shown. (See Tables S1−S6 of the Supporting Information for a complete list of all harmonic frequencies of all calculated systems.) ^{b} Electronic state and symmetry group. Bold label refers to structure shown in Figure 3. ^{c} A shoulder observed in the experimental spectrum is indicated by a (s). The symmetry of the vibrational mode, as well as its calculated oscillator strength, is given in parentheses.

Figure 3. Calculated structures of low energy isomers of $(Al_2O_3)_{1-4}(AlO)^+$ clusters and corresponding complexes with He-atoms. Bond lengths are given in angstroms.

Figure 4. Comparison of experimental IRVPD spectrum of $Al_5O_7{}^+ \cdot He_2$ (**Exp**) to simulated linear absorption spectra of the isomers **2A** and **2B** of $Al_5O_7{}^+ \cdot He_2$, depicted in Figure 3. The best agreement is obtained when assuming a 3:1 mixture of **2A** and **2B** (trace labeled **Mix**).

the Al−O bonds comprising the respective vibrational modes. (ii) The signal at higher energies (960−1000 cm^{-1}) results from stretching modes involving the shortest Al−O bonds (<1.7 Å), which are absent in $Al_3O_4{}^+$. The bands between 800−900 cm^{-1} correspond to stretching motions of Al−O bonds with predominantly medium bond lengths (1.7−1.8 Å). The vibrational modes below 800 cm^{-1} mainly involve displacement of the 3-fold coordinated O atom, which forms the longest (and weakest) Al−O bonds (>1.8 Å). Consequently, isomers **2A** and **2B** are characterized by similar IR spectra, despite their different geometries, because these structures exhibit a similar variety in Al−O bond lengths. (iii) The differences of calculated vibrational frequencies between $Al_5O_7{}^+ \cdot He_2$ and $Al_5O_7{}^+$ are much smaller than for $Al_3O_4{}^+$, due to weaker binding of the He atoms in the larger cluster. For $Al_5O_7{}^+ \cdot He_2$, a maximum shift of 5 cm^{-1} (compared to 20 cm^{-1} for $Al_3O_4{}^+$) is found for

vibrations involving the Al atoms bonded to He (see Table S2 of the Supporting Information).

$Al_7O_{10}{}^+$. The experimental spectrum of $Al_7O_{10}{}^+ \cdot He$ in the range from 530 to 1170 cm^{-1} is shown in Figure 5 (bottom trace). The strongest absorption is found at 996 cm^{-1}, followed by three bands of similar intensity at 953, 916, and 889 cm^{-1}. Many weaker absorption features are observed down to 560 cm^{-1}.

The DFT calculations yield two different structure types for $Al_7O_{10}{}^+ \cdot He$. For both, different variants exist, that differ either in the position of the He atom or constitute distorted versions of the same structure type. One type is a cage-like ion consisting of 4m and 6m rings (structures **3A** and **3B** in Figure 3; **3A** is a less symmetric variant of **3B**). The other type is more sheet-
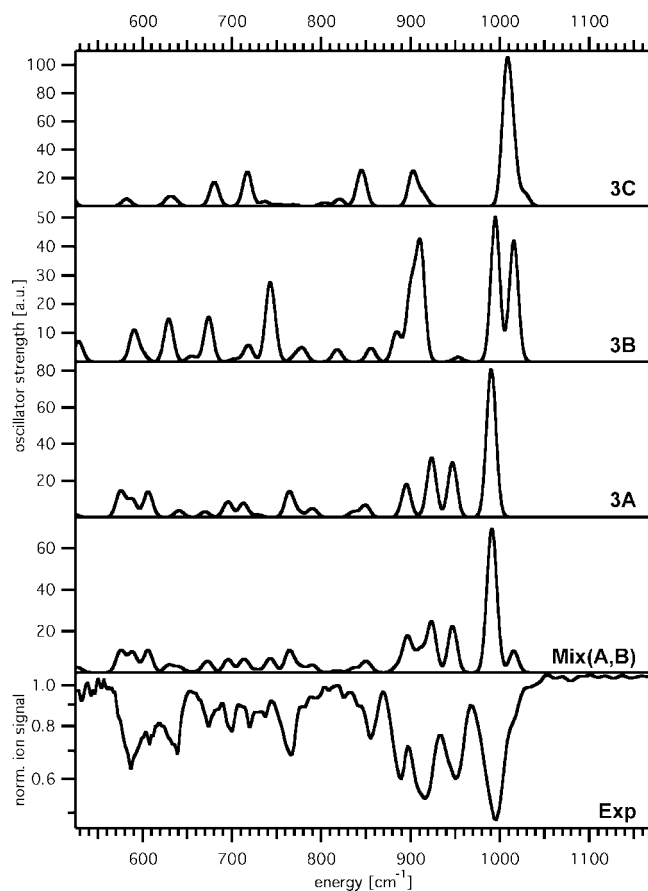
Figure 5. Comparison of experimental IRVPD spectrum of $Al_7O_{10}^+ \cdot He$ (**Exp**) to simulated linear absorption spectra of the isomers **3A**−**C** of $Al_7O_{10}^+ \cdot He$, depicted in Figure 3. The best agreement is obtained when assuming a 3:1 mixture of **3A** and **3B** (trace labeled **Mix(A,B)**).

Figure 6. Comparison of experimental IRVPD spectrum of $Al_9O_{13}^+ \cdot He$ (**Exp**) to simulated linear absorption spectra of isomer **4A**, depicted in Figure 3.

like, with two slightly buckled sheets forming an angle of about 90° (structure **3C** in Figure 3; more variants exist, but only the most stable structure is shown). At the B3LYP/def2-TZVP level, **3C** is the most stable structure, followed by **3B** (+19 kJ/mol) and **3A** (+23 kJ/mol). The differences in zero point energy are small in this case, the ZPE for **3A** and **3B** are almost identical and both are 0.5 kJ/mol higher than **3C** so that **3C** is minimally favored by ZPE. The energy differences remain nearly unchanged (+17 and +22 kJ/mol, respectively) upon increasing the size of the basis set (def2-QZVP). The stability sequence changes when wave function based methods are used instead of DFT (see Table S9 of the Supporting Information). At the MP2/def2-TZVP level, we find a minimal preference for **3B** followed by **3C** (+0.2 kJ/mol) and **3A** (+1 kJ/mol). Compared to B3LYP, the MP2 results show a slightly more pronounced basis set dependence. At the MP2/cc-pVQZ level **3B** remains the most stable ion, followed now by **3A** (+1 kJ/mol) and **3C** (+4 kJ/mol). Upon inclusion of core-valence correlation with the appropriate cc-pwCVQZ basis set the ordering remains the same: **3B**, **3A** (+1 kJ/mol), and **3C** (+7 kJ/mol). The relative stability of the two structure types is not only reversed between B3LYP and MP2, but a difference of more than 20 kJ/mol in relative energies is found.

Comparing the calculated harmonic frequencies and intensities of the three different structures (traces **3A**−**C** in Figure 5) with the experimental spectrum (trace **Exp** in Figure 5), reasonable agreement is found with the simulated spectrum of **3A**. The spectrum of **3C**, the global minimum at the B3LYP/def2-TZVP
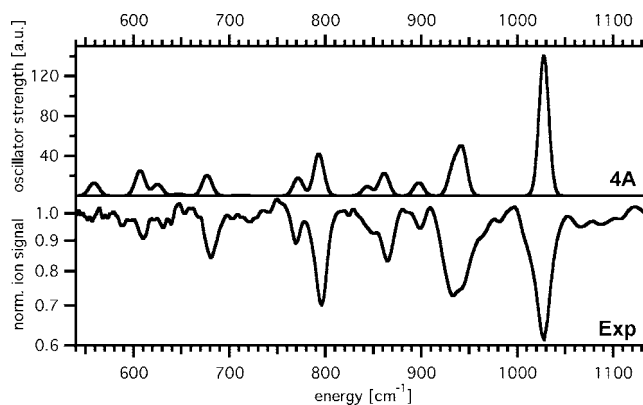
level, clearly does not fit the experimental spectrum, indicating that the preferred stability of **3A** and **3B** at the MP2 level is realistic. Still, MP2 predicts the highest stability for **3B**, while the agreement with the experimental spectrum is poorer than that for **3A**, in particular in the 850 to 1030 cm^{-1} range, where the strongest absorptions are observed. However, the energy difference between **3A** and **3B** is small; it is about 1 kJ/mol, well within the uncertainty range of MP2. The size of the ion and the low symmetry makes higher level calculations, e.g., CCSD(T), prohibitively expensive, so that a definitive answer about the global minimum cannot be given based on the calculations. Some indications exist that **3B** may contribute to the measured spectrum. The main differences compared to **3A** are the bands at 1016 cm^{-1}, 901 cm^{-1}, and 742 cm^{-1}. The first two might be visible in the experimental spectrum as shoulders and the last one could correspond to a peak at 738 cm^{-1}. Best agreement between experiment and theory is achieved if a 3:1 mixture of **3A** and **3B** (see trace **Mix(A,B)** in Figure 5) is assumed.

$Al_9O_{13}^+$. The global minimization search for $Al_9O_{13}^+$ yields only a single relevant structure; other structures have more than 70 kJ/mol higher energies. This structure is of the same symmetry (C_{3v}) as $Al_3O_4^+$, with which it shares some structural elements. It can be viewed as a conical $Al_3O_4^+ \cdot (Al_2O_3)_3$ cluster containing a 12m Al_6O_6 ring that is linked by three additional O atoms in Al−O−Al bridges to an $Al_3O_4^+$ unit comprising the tip of the cone. In the $Al_9O_{13}^+ \cdot He$ complex (structure **4A** in Figure 3), the He atom coordinates to a 3-fold coordinated Al atom sitting on the rim of the conical structure, leading to a lowering of the symmetry to C_s, but the distortion from the original 3-fold symmetry is small and its effect on the vibrational frequencies negligible (<2 cm^{-1}, see Table S6 in the Supporting Information). Given the laser resolution of ∼ 10 cm^{-1}, effects due to the messenger atom induced symmetry lowering cannot be resolved in this case.

The experimental IRVPD spectrum of $Al_9O_{13}^+ \cdot He$ (Figure 6, lower trace labeled **Exp**) shows a rich structure similar to the IRVPD spectra of the $n = 3$ and $n = 2$ ions. The most intense absorption is again found at the highest energy (1029 cm^{-1}) and shifted to the blue (+35 cm^{-1}) compared to the spectrum of the next smaller ion $Al_7O_{10}^+ \cdot He$. This band is assigned to the doubly degenerate O−Al−O stretching mode of $Al_9O_{13}^+$ involving the shortest Al−O bonds (1.69 Å) in the 12m ring at the rim of the cone. Figure 6 shows that the simulated spectrum reproduces all principal features of the experimental spectrum. However, some signals close to the noise level exist, e.g., at 700, 960

(shoulder), and 1070 cm^{-1} that have no counterpart in the simulated spectrum.

Conclusions

The presented results show that IRVPD spectroscopy combined with calculations of vibrational spectra, aided by a global minimization scheme, allows for a reliable identification of the global minimum structures for the $(Al_2O_3)_{1-4} \cdot AlO^+$ ions. Formation of the messenger atom complexes inside the gas-filled ion trap and not, as is usually done, directly following the laser ablation process, avoids the population of energetically higher-lying, relative minima on the potential energy landscape upon too rapid cooling in the supersonic expansion. For small ions, like $Al_3O_4^+$, where Al–He binding energies of ~1000 cm^{-1} and frequency shifts of up to 20 cm^{-1} between the complex and the bare ion are found, the presence of the messenger atoms needs to be considered explicitly, even when He atoms are used.

The measured IRVPD spectra appear somewhat richer in structure than the calculated linear absorption spectra. This is not unexpected, considering that the simulated spectra neglect effects resulting from anharmonicity, multiple photon absorption as well as a nonzero internal energy of the ions. However, the satisfactory agreement between the experimental and simulated spectra suggest that these effects are small and do not affect our overall interpretation.

In all four cases, the global minima differ considerably from bulk alumina structures. They all contain 3-fold coordinated aluminum, reminiscent of the undercoordinated Al-atoms found at the surfaces of alumina polymorphs, but not in their bulk structures. For $n = 2$ and $n = 3$, multiple structures of similar energy exist. While the characteristic features in IRVPD spectra can be assigned assuming a single isomer, a slightly better agreement is achieved, when the presence of two absorbing species is assumed. Our results indicate that in both cases, the cage-like isomer is more stable than the sheet-like one, a conclusion that is only supported by the MP2 and not the B3LYP calculations. For $n = 3$, two variants of the same structural motif with similar energy are predicted. However, the resolution of the experimental spectra is insufficient to deduce, if a single isomer, two stable isomers or a single one that is quickly interconverting via a low energy barrier transition state is actually observed.

For $n = 1$ and $n = 4$ only a single, exceptionally stable structure is found. The next member of a $(Al_2O_3)_n \cdot AlO^+$ series with C_{3v} symmetry should be $n = 10$, in which 6 O-atoms connect the $n = 4$ structural motif with a 24m $Al_{12}O_{12}$ ring,

forming the outer rim of a larger cone. Future studies must show if the characteristic conical motif, which has been identified for $n = 1$ and $n = 4$ in this work, persists also at larger cluster sizes. Its identification should be possible via the strong absorption band, characteristic of the short Al–O bonds (<1.7 Å) forming the rim of the conical structure, above 1000 cm^{-1}, a region in which the bulk modifications of Al_2O_3 show little to no absorption.

The methodology presented here for small aluminum oxide clusters can be readily transferred to related systems. The main experimental as well as theoretical limitation is the cluster size. First, the propensity of a cluster to bind a messenger atom under the present experimental conditions, which generally decreases with increasing cluster size, is the main experimental prerequisite. Second, the number of potential energy minimum structures increases nearly exponentially with cluster size and the time for each B3LYP optimization also increases. This makes the use of the genetic algorithm, which requires many B3LYP optimizations to find the global minimum energy structure, computationally too expensive. Finally, larger clusters that are not described well by DFT (see $Al_7O_{10}^+$ in the present case) cannot be studied, because wave function based calculations become prohibitive for larger clusters.

Supporting Information Available: Complete ref 46 (Appendix S1). Calculated vibrational frequencies and intensities of $Al_3O_4^+$ (Table S1), $Al_5O_7^+$ (Table S2), $Al_7O_{10}^+$ A (Table S3), $Al_7O_{10}^+$ B (Table S4), $Al_7O_{10}^+$ C (Table S5) and $Al_9O_{13}^+$ (Table S6) with and without helium atoms. Absolute and relative B3LYP/def2-TZVP energies for all clusters (Table S7). Absolute relative energies and energy differences with respect to the global B3LYP/def2-TZVP minimum for $Al_5O_7 \cdot He_2^+$ (Table S8) and $Al_7O_{10} \cdot He^+$ (Table S9). This material is available free of charge via the Internet at http://pubs.acs.org.

JA805216E